How the Primate Fornix Is Affected by Age

Alan Peters,* Claire Sethares, and Mark B. Moss

Department of Anatomy and Neurobiology, Boston University School of Medicine, Boston, Massachusetts 02118

ABSTRACT

The effects of age on nerve fibers and neuroglial cells in the fornix were examined in 25 rhesus monkeys between 4 and 33 years of age. There is no age-related change in the cross-sectional area of the fornix, but there is a significant loss of myelinated nerve fibers. The loss of myelinated nerve fibers is accompanied by a significant increase in the numbers of nerve fibers that show degeneration of their axons and alterations in myelin sheaths. Aging also brings about an increase in the frequency of profiles of paranodes, indicating that some of the nerve fibers are being remyelinated. Aging also affects neuroglial cells. Each type shows inclusions in their perikarya, and in the case of astrocytes and microglial cells some of these inclusions are phagocytosed myelin. Numbers of astrocytes and microglial cells do not appear to increase with age, but there is a 20% increase in oligodendrocytes. When correlations with cognitive impairments displayed by individual monkeys are examined, the decreased packing density of nerve fibers and the increasing frequency of nerve fibers with degenerating axons and of nerve fibers with altered myelin sheaths all correlate with increasing cognitive impairment. It is suggested that these correlations result from some disconnection of the hippocampus from the thalamus, septal nuclei, and medial frontal cortex and from reductions in the conduction velocity brought about by the shorter internodal lengths of remyelinated nerve fibers in the fornix. J. Comp. Neurol. 518:3962–3980, 2010.

INDEXING TERMS: *Macaca mulatta*; myelin degeneration; nerve fiber loss; aging neuroglial cells; cognitive assessment

It is now generally agreed that there is not a significant loss of cortical neurons from the brains of normally aging human and nonhuman primates (see, e.g., Morrison and Hof, 1997; Peters et al, 1998a; Freeman et al., 2008), although there may be some focal loss of neurons from specific areas of prefrontal cortex (Smith et al., 2004). However, this does not mean that cortical neurons are unaffected by age, because there is a loss or regression of some of their dendritic branches, and the remaining dendrites lose some of their spines (see, e.g., Jacobs et al., 1997; Peters et al., 1998b; Duan et al., 2003). This probably contributes to the age-related loss of some excitatory and inhibitory synapses from cortex (Peters et al., 1998b, 2001b, 2008). Myelinated axons are also altered by age, as was pointed out several years ago when it was found that, in old humans and monkeys, white matter shows a decreased intensity of staining (see, e.g., Lintl and Braak, 1983; Kemper, 1994). The underlying reason for this age-related myelin staining pallor is not clear, but it is now known that with age some nerve fibers are lost from white matter and that some myelin sheaths undergo structural changes.

The age-related changes in the structure of myelin sheaths appear to be ubiquitous; we have encountered them in the cerebral cortex (Peters et al., 2000; Peters and Sethares, 2002), substantia nigra (Siddiqi and Peters, 1999), splenium of the corpus callosum (Peters and Sethares, 2002), optic nerve (Sandell and Peters, 2001), and anterior commissure (Sandell and Peters, 2003). The question of whether there is a general loss of myelinated nerve fibers during normal aging is more difficult to answer. For example, MRI studies are equivocal. Some studies, such as those of Albert (1993) and Guttman et al. (1998) on normal aging humans and of Lai et al. (1995) and Wisco et al. (2008) on monkeys, report a significant loss of white matter volume from the cerebral hemispheres, but there are other MRI studies, such as those of Pfefferbaum et al. (1994) on humans and Andersen et al. (1990) on monkeys, that conclude that there is little decrease in white matter volume and that any volume loss is mainly from gray matter. On the other hand, there

Grant sponsor: National Institutes of Health; National Insitute on Aging; Grant number: Program Project Grant 1PO AG 00001; Grant number: R37 AG17609.

*CORRESPONDENCE TO: Dr. Alan Peters, Department of Anatomy and Neurobiology, Boston University School of Medicine, 72 East Concord Street, Boston, MA 02118. E-mail: apeters@cajal-1.bu.edu

Received March 2, 2010; Revised April 7, 2010; Accepted April 25, 2010
DOI 10.1002/cne.22434
Published online May 20, 2010 in Wiley InterScience (www.interscience.wiley.com)

seems to be a general consensus among those who employ diffusion tensor MRI, which uses diffusional anisotropy as a marker of white matter integrity, that white matter is altered with age (see, e.g., O'Sullivan et al., 2001; Madden et al., 2004).

The most direct evidence of loss of myelinated nerve fibers from white matter in normal aging comes from stereological studies. Pakkenberg and Gundersen (1997) used stereology to examine age changes in human cerebral hemispheres and determined that, even though the volume of gray matter decreases by 12%, the loss of nerve fibers is greater, being 28%. A followup study by Tang et al. (1997) examined the myelinated nerve fibers in the white matter of human cerebral hemispheres and concluded that the decrease in white matter volume is associated with a 27% overall loss from the total length of myelinated nerve fibers. A more recent, and expanded, study by Marner et al. (2003), with 36 normal human subjects, reinforced this conclusion and showed that the white matter loss from human cerebral hemispheres is almost 23%, and between the ages of 20 and 80 the overall reduction of nerve fiber length is 45%.

In our studies of the effects of age on myelinated nerve fibers in the cerebral cortex of the rhesus monkey, we have observed no significant loss of nerve fibers from the vertical myelinated bundles in primary visual cortex (Nielsen and Peters, 2000), but, in contrast, we have found myelinated nerve fibers to be lost from white matter tracts such as optic nerves (Sandell and Peters, 2001), anterior commissure (Sandell and Peters, 2003), and corpus callosum (unpublished data) of the rhesus monkeys. Each of these structures is a well-circumscribed bundle of nerve fibers in which it is possible to make exact nerve fibers counts, but they differ in that, whereas the optic nerve originates from neurons in a peripheral sensory organ, the nerve fibers of the anterior commissure and corpus callosum originate from neurons in the cerebral cortex.

One other well-circumscribed bundle of myelinated nerve fibers in the brain is the fornix, which is the principal projection bundle from the hippocampus to other components of the Papez circuit in the limbic system. In some species, such as the rabbit and rat, two fornices have been described. One is the subcallosal fornix, which remains ventral to the corpus callosum, and the other is the dorsal fornix, which is a small group of fibers that runs cranially in the substance of the corpus callosum. In primates, a dorsal fornix does not exist (Poletti and Creswell, 1977), so only the subcallosal fornix, simply referred to as the *fornix*, is present.

In monkey, efferent nerve fibers that originate from the pyramidal cells of the hippocampus and subiculum pass into the fornix, which reciprocally connects the hippocampus to such structures as the mammillary body; the septal area; several subcortical areas, including the anterior and lateral nuclei of the thalamus, the hypothalamus, and the ventral striatum; as well as medial frontal cortex (Poletti and Creswell, 1977; Swanson and Cowan, 1977; Rosene and Van Hoesen, 1987; Johnston and Amaral, 1998). Most of the fibers in the fornix pass behind the anterior commissure to form the postcommisural fornix. These fibers originate in the subiculum and terminate in the mammillary body and in the anterior nucleus of the thalamus. Other fibers, which originate in both the hippocampus and the subiculum, form the precommisural fornix and terminate in the septal nuclei, hypothalamus, and medial frontal cortex (Rosene and Van Hoesen, 1987). The present study examines the effects of age on the nerve fibers and glial cells in the fornix of the rhesus monkey before it splits into its pre- and postcommissural components.

MATERIALS AND METHODS

Animals

Segments of the fornix were taken from the brains of 25 rhesus monkeys (*Macaca mulatta*) ranging from 4 to 33 years of age. Nine of the monkeys between 4 and 10 years of age were considered to be young, seven monkeys between 12 and 20 years of age were considered to be middle-aged, and the other nine monkeys, 22 years old and over, were considered to be old. The ages of these monkeys and their sexes are given in Table 1.

Details of the protocol for fixing the brains of these monkeys have been given in earlier publications (see, e.g., Peters et al., 1994). All procedures regarding the care and death of these animals was approved by the Institutional Animal Care and Use Committee of Boston University School of Medicine, in accordance with the NIH *Guide for the care and use of laboratory animals*. In summary, the monkeys were preanesthetized with ketamine (6.5mg/kg). Sodium pentobarbital was then administered intravenously (approximately 35–45 mg/kg) until a state of areflexia was attained. The monkeys were intubated into the trachea and artificially respired with a mixture of CO_2 and O_2. The chest was opened, and the monkeys were perfused intraaortically with a warm solution of 1.25% glutaraldehyde and 1.0% paraformaldehyde in 0.1 M cacodylate or phosphate buffer at pH 7.4. All efforts were made to minimize the numbers of monkeys used and their suffering.

On completion of the perfusions, the brains were removed, the brainstem was cut off, and the cerebral hemispheres were separated in the midsagittal plane. One hemisphere was then fixed further by immersion in a cold solution of 2% paraformaldehyde and 2.5%

TABLE 1.
Number of Nerve Fibers in Fornix: Light Microscopic Analysis

Animal number	Sex	Age (years)	Area (mm^2)	Density of fibers (per 100 μm^2)	Total myelinated fibers ($\times 10^5$)	CII
AM 58	M	4	2.13	51.4 ± 19.6	11.0 ± 4.2	No data
AM 7	M	5	2.75	37.1 ± 18.9	10.2 ± 5.2	No data
AM 76	F	6	2.57	52.5 ± 16.9	13.5 ± 4.4	0.08
AM 77	F	6	2.18	52.9 ± 18.7	11.5 ± 4.1	2.27
AM 129	F	7	3.11	45.4 ± 16.3	14.1 ± 5.1	1.87
AM 130	F	8	1.98	50.0 ± 14.4	9.9 ± 2.8	1.28
AM 47	M	9	2.54	39.9 ± 18.9	10.1 ± 4.8	0.51
AM 96	F	9	2.18	47.1 ± 18.6	10.3 ± 4.0	2.12
AM 53	M	10	2.32	38.7 ± 11.4	9.0 ± 2.6	0.32
Means			2.42 ± 0.36	46.1 ± 17.1	11.1 ± 4.1	
AM 42	M	12	2.55	44.3 ± 14.6	11.3 ± 3.7	0.95
AM 140	M	12	2.89	52.0 ± 18.1	15.0 ± 5.2	No data
AM 144	M	15	2.69	49.2 ± 15.5	13.2 ± 4.2	0.42
AM 221	F	18	2.54	42.3 ± 12.5	11.4 ± 3.4	2.71
AM 209	M	19	3.14	42.4 ± 13.2	13.3 ± 4.1	0.8
AM 101	M	19	2.70	40.3 ± 17.4	12.1 ± 4.7	4.21
AM 133	M	20	3.01	40.0 ± 19.4	12.0 ± 5.9	2.46
Means			2.79 ± 0.23	45.1 ± 15.2	12.7 ± 4.2	
AM 178	F	22	3.02	44.2 ± 17.8	13.3 ± 5.4	6.2
AM 19	F	25	2.87	27.6 ± 12.5	7.9 ± 3.6	1.98
AM 100	F	25	2.26	40.3 ± 15.3	9.1 ± 3.4	3.59
AM 62	M	27	2.88	31.3 ± 13.7	9.0 ± 3.9	3.81
AM 27	M	28	2.56	43.0 ± 18.6	11.0 ± 4.7	1.24
AM 23	F	32	1.94	48.7 ± 18.0	9.5 ± 3.5	6.75
AM 41	F	32	2.16	46.2 ± 20.1	10.0 ± 4.3	4.51
AM 91	M	32	2.61	34.7 ± 19.4	9.1 ± 5.1	0.25
AM 18	M	33	2.74	27.9 ± 17.0	7.6 ± 4.7	No data
Means			2.56 ± 0.38	38.2 ± 16.9	9.6 ± 9.3	

glutaraldehyde in 0.l M cacodylate or phosphate buffer until needed for the present study. The other hemisphere was frozen, sectioned in the frontal plane, and a set of Nissl stained sections was prepared.

Tissue preparation

To remove pieces of fornix for light and electron microscopic examination, the hemisphere was oriented to show the midsagittal plane, which had been exposed by the bisection of the corpus callosum. A razor blade cut was made in the frontal, or transverse, plane at a level midway between the rostral and caudal poles of the bisected thalamus. The cut passed through the thalamus, the corpus callosum, and the body of the fornix present on that side of the brain. A second and parallel cut was then made at a level about 3 mm rostral to the first one. This exposed the fornix, which at this level is in the lateral ventricle, hanging suspended beneath the corpus callosum. Essentially, this level corresponds to level 2C in the illustrations of Demeter et al. (1985). The slice of tissue between the cuts was taken, and a block containing the fornix, part of the corpus callosum, and the superior portion of the thalamus was removed. The block was then osmicated, dehydrated in an ascending series of alcohols, and embedded in Araldite.

For examination of the effects of age on its nerve fibers and glial cells, the embedded fornix was sectioned in the transverse plane, so that its nerve fibers were cross-sectioned. Semithick (1 μm) sections of the entire fornix were first taken and stained with toluidine blue for light microscopy. These sections were used to determine the effects of age on the total number of nerve fibers contained in the fornix and on the population of neuroglial cells. For electron microscopy, the block was trimmed so that the thin sections contained only the lateral portion of the fornix. This was necessary because an entire cross-section of the fornix is too large to fit onto an electron microscope grid. All thin sections were stained with uranyl acetate and lead citrate and used to determine proportions of myelinated and unmyelinated nerve fibers, the effects of age on the sheaths and axons of the myelinated nerve fibers, the frequency of profiles of nodes and paranodes, and the age-related changes in the frequency of neuroglial cells.

Nerve fiber counts by light microscopy

An estimate of the total number of nerve fibers in the fornix on the one side of the brain was obtained by examining the semithick sections stained with toluidine blue, using the Bioquant BQ-TCX-95 system (R & M biometrics,

Nashville TN) and a motorized stage. The image was projected onto a video monitor.

First, the cross-sectional area of the fornix was determined with a ×4 objective. In four cases, the complete fornix on one side was not included in the tissue block used to count nerve fibers. However, because the other hemisphere had been sectioned in the frontal plane and Nissl-stained sections prepared by Dr. Douglas Rosene, it was possible to match the semithick sections of the fornix with the Nissl-stained sections taken at the same level on the other side of the brain and to determine how much of the fornix was missing from our sections. This allowed the true cross-sectional areas of such fornices to be ascertained.

Second, each section was viewed with a ×100 oil immersion objective (NA 1.40) to determine the packing density of the nerve fibers. The counting was carried out by one of the authors (C.S.). A computer was used to generate the counting boxes (10 μm × 10 μm), spaced center-to-center in a randomly placed 100 μm × 100 μm grid pattern; to move the stage; to project the counting box onto the video screen; to mark the profiles that were counted; to tally the counts; and to calculate the cross-sectional area of the fornix. In the counting box, all myelinated nerve fiber profiles were counted if they did not intersect the two forbidden margins of the box. For each fornix, the counting parameters were determined empirically to yield coefficients of error (CE = SEM/mean), which were within the 10% recommended by West and his colleagues for stereological analyses (West et al., 1996; Howard and Reed, 1998).

However, it must be pointed out that counting myelinated nerve fibers in the fornix by light microscopy presents some difficulties that can lead to inaccuracies. To obtain accurate counts of myelinated nerve fibers cut in cross-section, the circular image of the stained myelin sheath must be obvious, and in the fornices of old monkeys the morphology of the sheaths can be distorted by the inclusion of dense cytoplasm in the sheaths, cytoplasm that in toluidine blue-stained sections has the same dark blue color as the myelin. This can make it difficult to know whether a profile comprises only one sheath or two sheaths juxtaposed. Another problem is that, even with a high-power objective, it is often difficult visually to separate the profiles of two small-diameter fibers with thin sheaths when they are touching each other. Nevertheless, to obtain estimates of the total numbers of nerve fibers in the fornix, it is necessary to carry out light microscopic analyses, because a section though an entire fornix is too large to fit onto an electron microscopic grid.

To obtain estimates of the total number of nerve fiber profiles, the mean number of profiles per square millimeter was multiplied by the cross-sectional area of the fornix. The data derived from light microscopy are given in Table 1.

Quantitative analyses of nerve fibers by electron microscopy

The thin cross-sections of the lateral portion of the fornix were mounted on 200 mesh grids, and, after they had been examined to ascertain that the quality of preservation was acceptable, electron micrographs were taken at an initial magnification of ×5,000. The electron micrographs covered the entire area of the thin section. They were taken in a systematic manner, so that micrographs were taken of nerve fibers in every third opening along every third row of the 200 mesh grid. Essentially, this means that micrographs were taken of nerve fibers in every ninth hole in that portion of the grid covered by the thin section of the fornix. In taking these micrographs, blood vessels and the cell bodies of neuroglial cells were avoided, so that fields containing only nerve fibers were photographed.

The electron microscopic negatives were printed to a final magnification of ×12,500, and with a counting box the numbers of myelinated and unmyelinated nerve fibers per unit area were determined. This entailed examining at least 10 prints from each fornix and counting at least 1,000 myelinated nerve fibers. On these same prints, assessments were also made of the proportion of profiles of myelinated nerve fibers sectioned through internodes, paranodes, and nodes of Ranvier. The criteria for recognizing profiles of these parts of myelinated nerve fibers are well established and are given by Peters et al. (1991b) and Peters and Sethares (2003). In addition, determinations were made of the numbers of profiles of myelinated nerve fibers that showed age-related alterations in the morphology of their sheaths or degeneration of their axons. These data are presented in Table 2.

Neuroglial cell counts by light microscopy

Neuroglial cells were counted from the semithick toluidine blue-stained plastic sections. The Bioquant system was used with a ×60 oil immersion objective. A 40 μm × 40 μm counting box was used, and the counting boxes were spaced 200 μm apart. The objects counted were the profiles of astrocytes, oligodendrocytes, and microglial cells that displayed their nuclei. Two observers (A.P. and C.S.) working together made the counts. It was assumed that a sufficient number of counts had been made when the coefficients of error (CE = SEM/mean) for the numbers of profiles of astrocytes and of oligodendroglial cells counted were again 10% or below. Because microglial cells are so sparse, no attempt was made to make sufficient counts of these cells to attain a 10% CE,

TABLE 2.
Nerve Fibers in the Fornix: Electron Microscopic Analysis

Animal number	Sex	Age (years)	Myelinated fibers per 100 μm^2	Myelinated fibers: Percentages				Totals: Percentages		CII
				Internodes	Paranodes	Nodes	Altered sheaths	Altered axons	Myelinated	Unmyelinated	
AM 58	M	4	69	93.4	5.6	1.0	0.2	0	62.1	37.9	No data
AM 7	M	5	61	95.2	4.2	0.6	0.1	0.1	58.0	42.0	No data
AM 76	F	6	66	92.8	6.2	1.0	0.1	0	61.4	38.6	0.08
AM 77	F	6	64	94.8	4.1	1.0	0.3	0	55.8	44.2	2.27
AM 129	F	7	60	94.5	4.3	1.2	0.3	0	64.8	35.2	1.87
AM 130	F	8	59	94.4	4.8	0.8	0.1	0	71.3	28.7	1.28
AM 47	M	9	64	94.6	4.5	0.9	0.1	0	62.5	37.5	0.51
AM 96	F	9	68	93.0	6.2	0.8	0.7	0	59.2	40.8	2.12
AM 53	M	10	57	92.9	6	1.1	0.9	0.1	68.6	31.4	0.32
Means			63 ± 4	94.0%	5.1%	0.9%	0.3%	0%	62.6%	37.4%	
AM 42	M	12	61	92.4	6.6	1.0	1.8	0	68.4	31.6	0.95
AM 140	M	12	60	93.0	6.0	1.0	0.8	0	61.5	38.5	No data
AM 144	M	15	55	92.3	6.8	0.8	2.4	0.3	58.9	41.1	0.42
AM 221	F	18	49	93.2	5.8	1	3.7	0.4	56	44	2.71
AM 209	M	19	55	93.3	5.9	1.2	3.4	0.2	71.5	28.5	0.80
AM 101	M	19	49	92.2	6.7	1.1	2.2	0	52.9	47.1	4.21
AM 133	M	20	50	93	6.1	0.9	2.7	0.3	58.1	41.9	2.46
Means			54 ± 5	92.6%	6.3%	1.0%	2.4%	0.2%	61.0%	39.0%	
AM 178	F	22	46	91.8	7.0	1.2	2.4	0.4	69.2	30.8	6.2
AM 19	F	25	39	90.1	9.0	0.9	4.7	0.2	58.4	41.6	1.98
AM 100	F	25	46	92.5	6.3	1.2	3.2	0.2	65.0	35.0	3.59
AM 62	M	27	53	90.0	8.2	1.2	3.9	0.2	54.5	45.5	3.81
AM 27	M	28	51	92.6	6.4	1.0	4.4	0.2	63.0	37.0	1.24
AM 23	F	32	45	92.4	6.8	0.7	3.6	0.4	53.1	46.9	6.75
AM 41	F	32	46	93.3	6	0.7	4.8	0.5	54.7	45.3	4.51
AM 91	M	32	46	91.9	7	1.1	2.8	0.2	55.7	44.3	0.25
AM 18	M	33	47	91.4	7.8	0.9	1.7	0.4	43.9	56.1	No data
Means			47 ± 4	91.7%	7.2%	1.0%	3.5%	0.3%	57.5%	42.5%	

so that most of the microglial cell counts were at the 20% level. From the counts, assessments were made of the numbers of neuroglial cell profiles per unit area. These data are presented in Table 3.

Behavioral testing

The behavioral tests used to determine the cognitive status of individual monkeys have been described in detail in earlier publications (e.g., Peters et al., 1996; Herndon et al., 1997; Moss et al., 1999; Killiany et al., 2000). The battery of tests included three visual recognition tasks: the delayed nonmatching to sample (DNMS) task, a test of rule learning; the DNMS task with a 2-minute delay, a test of short-term memory; and the delayed recognition memory span (DRST) task, which tests for working memory. From the scores achieved on these tasks, an overall measure of cognitive impairment (Peters et al., 1998b), the cognitive impairment index (CII), was derived. Specifically, the individual scores on the three behavioral tasks are transformed to scores normalized to a population of 53 adult rhesus monkeys, as described by Herndon et al. (1997), and a composite score, the cognitive performance index, is derived. This is a practical index of global ability and its inverse, the CII, is a measure of cognitive impairment. When this index was first derived, the number of trials to criterion was used as the measure of performance on the DNMS task. As more data were collected, the number of errors to criterion proved to be a more sensitive measure of performance, so this was substituted for the number of trials to criterion that had been used earlier as the index of performance on the basic DNMS task. This substitution led to a recalculation of some of the CII scores, so that some of the CII scores given in Table 1 are slightly different from those given in earlier publications from our group. Essentially, the higher the CII, the more a monkey is cognitively impaired. The CII values for those monkeys that had been tested are given in the Tables.

Statistical analyses

We performed a series of statistical analyses to examine the relationships among age, the morphological variables, and the behavioral variables of interest. In our primary analyses, we examined the association between morphological measures (myelinated nerve fibers density, percentage paranodal profiles, percentage nodes, percentage altered sheaths, and percentage altered axons)

TABLE 3.
Neuroglial Cells

Animal number	Sex	Age (years)	No. of cells/1 mm^2			CII
			Oligodendrocytes	Astrocytes	Microglia	
AM 58	M	4	1,082	273	40	No data
AM 7	M	5	810	315	92	No data
AM 76	F	6	940	179	84	0.08
AM 77	F	6	938	206	72	2.27
AM 129	F	7	1,052	202	57	1.87
AM 130	F	8	1,092	231	54	1.28
AM 47	M	9	719	161	37	0.51
AM 96	F	9	874	219	49	2.12
AM 53	M	10	804	219	43	0.32
Means			923 ± 133	223 ± 47	59 ± 20	
AM 42	M	12	787	164	38	0.95
AM 140	M	12	1,052	202	57	No data
AM 144	M	15	1,039	142	88	0.42
AM 221	F	18	927	167	58	2.71
AM 209	M	19	1,028	187	76	0.80
AM 101	M	19	878	205	85	4.21
AM 133	M	20	1,057	213	52	2.46
Means			967 ± 105	183 ± 26	65 ± 17	
AM 178	F	22	1,019	218	30	6.20
AM 19	F	25	798	169	46	1.98
AM 100	F	25	869	195	88	3.59
AM 62	M	27	1,108	176	75	3.81
AM 27	M	28	1,227	241	69	1.24
AM 23	F	32	1,170	255	101	6.75
AM 41	F	32	1,350	289	96	4.51
AM 91	M	32	1,458	243	90	0.25
AM 18	M	33	1,125	222	27	No data
Means			1,125 ± 211	223 ± 39	69 ± 27	

and age using both Pearson correlations analyses, and piecewise linear regression models performed by Dr. Howard Cabral. The latter approach was employed to determine whether there were significant nonlinear aspects to these relationships that could be captured by fitting slopes with prespecified age intervals. For these intervals, "young" is defined as being $\leq$10 years of age, "middle-aged" is defined as $>$10 but $<$20 years of age, and the "old" is defined as $\geq$20 years of age. For correlations of the data with behavioral variables, we employed the Pearson correlation using a linear fit.

Image processing

Electron micrographs were taken with a JEOL 100S electron microscope (JEOL USA, Peabody, MA). Representative electron microscopic negatives were scanned on an Epson Perfection V700 photoscanner using the Epson Perfection V700/V750 plug-in software for Adobe Photoshop CS v.8.0 software (Adobe Systems, San Jose, CA). Light micrographs were taken with a Nikon Coolpix 995 digital camera attached to a Zeiss Axioskop light microscope. Light and electron microscopic images were adjusted for exposure and sharpened in Photoshop.

RESULTS

The fornix connects the hippocampus with a number of subcortical areas. It begins in the inferior horn of the lateral ventricle, then loops around the posterior surface of the thalamus, and in the body of the lateral ventricle it comes to lie on top of the thalamus. As the fornix passes rostrally, the shape of its profile gradually changes, so that it becomes thicker and more compact. In the body of the lateral ventricle, where our blocks of tissue were taken, its medial surface fuses with that of the matching fornix in the other hemisphere, and in the midline they both become attached to the underside surface of the corpus callosum (Fig. 1). As it progresses rostrally, the lateral compression of the fornix continues so that it becomes a more rounded bundle. This occurs just before the fornices of the two sides separate from each other to form the anterior columns, which penetrate the thalamus and pass toward the mammillary bodies (see Demeter et al., 1985).

Even though the segments of fornix that we examined were taken from the same location, the shapes of their cross-sections varied from monkey to monkey. In some cases the cross-sectional profile of the fornix is rather

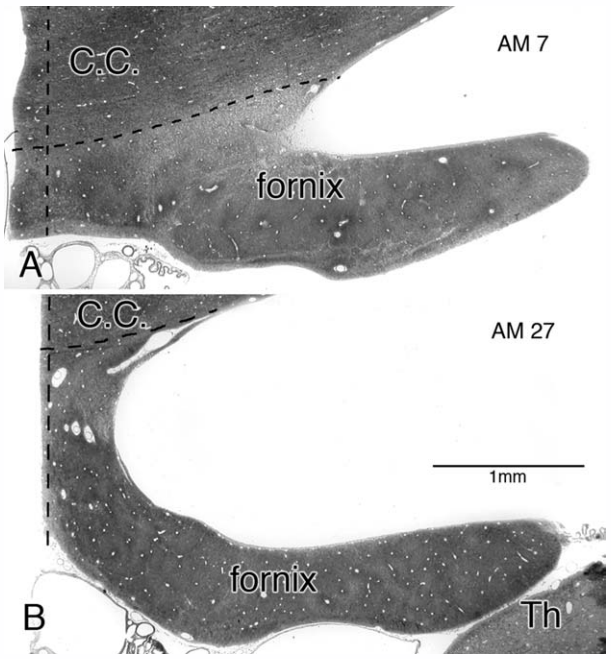

Figure 1. A,B: Light microscope pictures of semithick plastic sections of the fornix stained with toluidine blue to show examples of the variation in the shape of the transversely sectioned fornix at the level of the middle of the thalamus. The boundary between the fornix and the corpus callosum (c.c.) is shown by the horizontal dotted line, and the midline is given by the vertical dotted line. In B, part of the thalamus (Th) is visible. Scale bar = 1 mm.

squat, with only a short lateral protrusion (Fig. 1A); in other examples, it has a more ribbon-like profile (Fig. 1B). In each case, however, at the level from which our blocks of tissue were taken, the fornices of the two sides had joined in the midline and become attached to the underside surface of the corpus callosum (Fig. 1). In some examples, the attachment beneath the corpus callosum is extensive (Fig. 1A), but, in other cases, the attachment is through a thin vertical sheet, which is presumed to represent the septum pellucidum; in still other examples, the subfornical organ is apparent in the midline on the underside surface of the body of the fornix. It should be emphasized that, even though the profile of the fornix varies, this does not affect counts of the numbers of nerve fibers contained in the fornix; even though some commissural fibers exist (Demeter et al., 1985), no nerve fibers leave or enter the fornix until its anterior columns penetrate the septum.

Light microscopy

In semithick transverse sections stained with toluidine blue (Fig. 2), the myelinated nerve fibers that make up the fornix are cross-sectioned, and the majority of them are small in diameter (1–1.5 μm). However, throughout, there is a scattering of groups of larger diameter fibers (about 3 μm), and these become more frequent toward the midline. Along the border with the corpus callosum, the large fibers are quite loosely packed, and as a consequence the staining of this portion of the fornix is usually pale (see Fig. 1A).

The border between the fornix and the corpus callosum is easy to discern, because the nerve fibers of the fornix are passing in a rostrocaudal direction, whereas those of the corpus callosum are passing transversely, between the two hemispheres. The medial border between the fornices on each side of the brain can also be readily defined, because in the midline there is a paucity of nerve fibers and an indentation in the lower surface of the fornix.

In addition to nerve fibers, the fornix contains neuroglial cells, most of which are oligodendrocytes (Fig. 2, O). However, islands of nerve cells may also be present, together with the dendrites extending from them. Usually, these dendrites are in bundles passing parallel to the nerve fibers. To complete the picture, it should also be mentioned that the upper surface of the fornix, facing the corpus callosum, is covered by ependymal cells, whereas the lower surface, which faces the thalamus, is covered by an astrocytic limiting membrane, outside of which is the pia.

In semithick toluidine blue-stained sections examined by light microscopy, few differences can be seen between the fornices of the young (Fig. 2A) and old (Fig. 2B) monkeys, beyond the fact that the nerve fibers in old monkeys sometimes appear to be more loosely packed, and age-related balloons of myelin may be evident (Fig. 2B, thin arrows) as well as some nerve fibers with thick sheaths and others in which the axon has a dark cytoplasm (Fig. 2B, thick arrow).

Cross-sectional area of the fornix

As shown in Table 1 and in Figure 3A, when the data for male and female monkeys are pooled, it is evident that there is no significant change in the cross-sectional area of the fornix with age ($r = 0.082$: NS).

Counts of myelinated nerve fibers

Light microscopy

Despite the overall lack of change in the cross-sectional area of the fornix with age, the light microscopic analysis of the mean packing density of myelinated nerve fibers using the Bioquant system shows that there is a decrease in the mean packing density of myelinated nerve fibers with age (Table 1). Thus, as determined by light microscopy, the mean density of myelinated nerve fibers per 100 μm^2 in young monkeys is 46.1 ± 17.1, whereas in middle-aged monkeys it is 45.1 ± 15.2, and

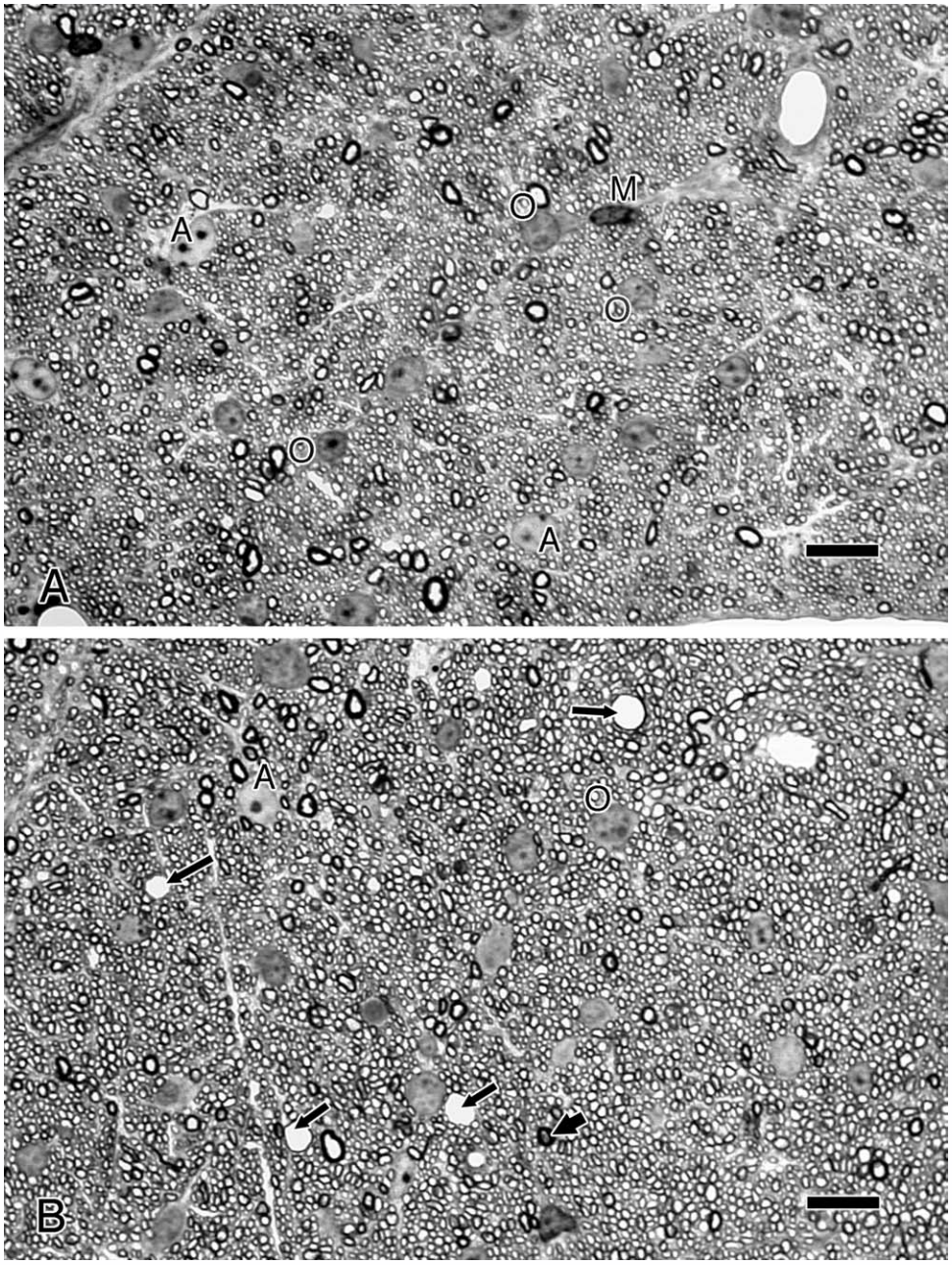

Figure 2. High-power light micrographs of semithick plastic sections of fornices stained with toluidine blue. **A** is from a 7-year-old monkey (AM 129) and shows an area containing many small-diameter nerve fibers, between which are groups of medium-sized and large fibers. **B** is from a 25-year-old monkey (AM 100). The field contains a relatively homogeneous population of medium-sized fibers, and in the field are several myelin balloons (thin arrows) and at least one nerve fiber that contains a dark axon (thick arrow). Between the nerve fibers are neuroglial cells, the most common of which are the oligodendrocytes (O), which have rounded nuclei with patchy chromatin. In contrast, astrocytes (A) have larger and pale nuclei, whereas the least common neuroglial cells, the microglia (M), have darkly staining, irregular nuclei. Scale bars = 10 μm.

in old monkeys it is 38.2 ± 16.9 (Fig. 3C). Consequently, when the total number of myelinated nerve fibers in the fornix is calculated, it is found that in young monkeys there are about 11.1×10^5 nerve fibers, whereas in old monkeys the mean number is reduced to 9.6×10^5, and there is a significant correlation between reduced numbers of nerve fibers and age (Fig. 3B; $r = 0.436$, $P = 0.0295$). Thus, when young and old monkeys are compared, the overall loss of nerve fibers is about 25%. Although the packing density of nerve fibers in the middle-aged monkeys is less than that in the young ones, when young and middle-aged monkeys are compared

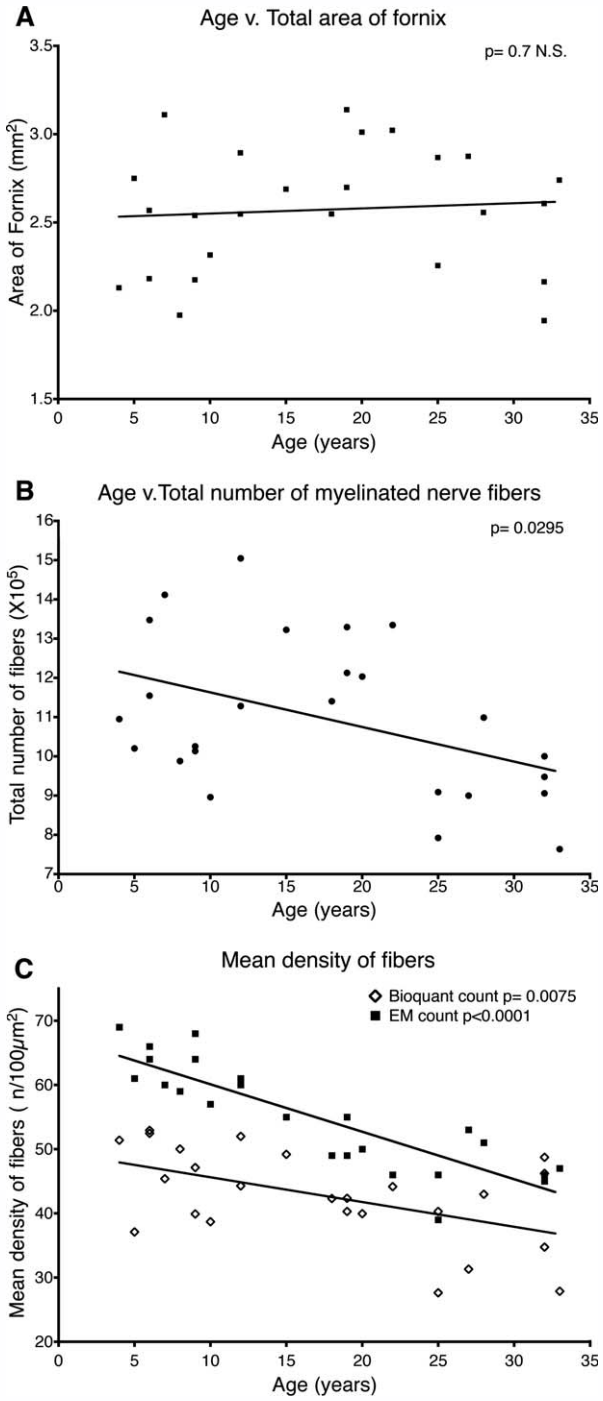

Figure 3. Graphs of changes in morphology as a function of age. **A:** Graph of the cross-sectional area of the fornix as a function of age. **B:** Graph of the total numbers of myelinated nerve fibers in the fornix as a function of age, as determined by light microscopy. **C:** Mean density of myelinated nerve fiber profiles per 100 μm^2 as a function of age. The plots give a comparison of the packing densities of nerve fibers as determined by light (Bioquant) and electron microscopy.

there appears to be an increase in total numbers of nerve fibers in middle-aged monkeys. This occurs because the mean cross-sectional areas of the fornices in the middle-aged monkeys in our sample are somewhat larger than those of the young monkeys (Table 1).

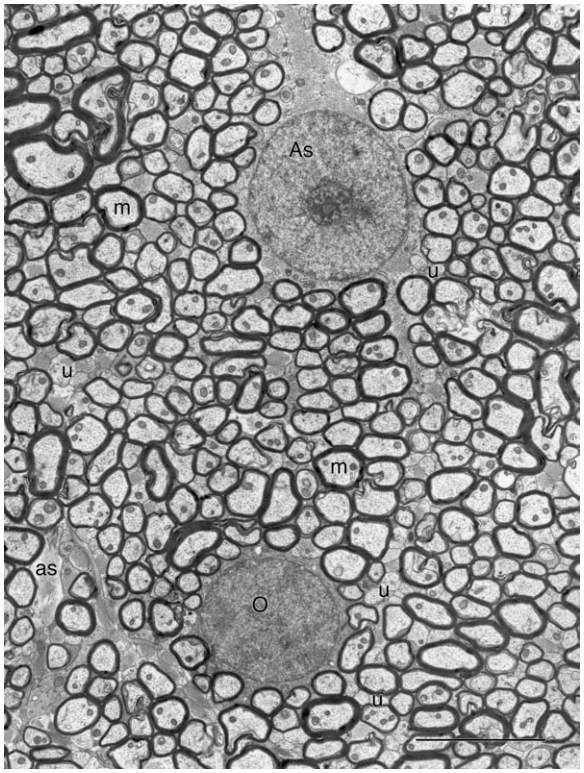

Figure 4. Low-power electron micrograph from the fornix of a 7-year-old monkey (AM 130). The myelinated nerve fibers (m) are closely packed, and between them are some unmyelinated nerve fibers (u) and the processes of astrocytes (as). There are two neuroglial cells in the field, an oligodendrocyte (O) and an astrocyte (As). Scale bar = 5 μm.

Electron microscopy

Analysis of electron micrographs from the lateral half of the fornix (Fig. 3C) confirms that there is a decrease in the packing density of myelinated nerve fiber in the fornix with increasing age ($P < 0.0001$). However, it should be noted that for young monkeys the packing density of nerve fibers per 100 μm^2 as determined by electron microscopy (Table 2) is about 35% higher than the values obtained from the light microscopic analysis (Table 1), and for middle-aged and old monkeys the differences between the light and electron microscopic counts are 20% and 23%, respectively (see Fig. 3C). The main reasons for these differences are as follows. The counts made by light microscopy were made over the entire extent of the fornix, including the medial portion, where the myelinated nerve fibers are often widely separated. Also, as pointed out in Materials and Methods, there are problems in obtaining accurate counts of profiles of nerve fibers with small-diameter fibers and thin sheaths,

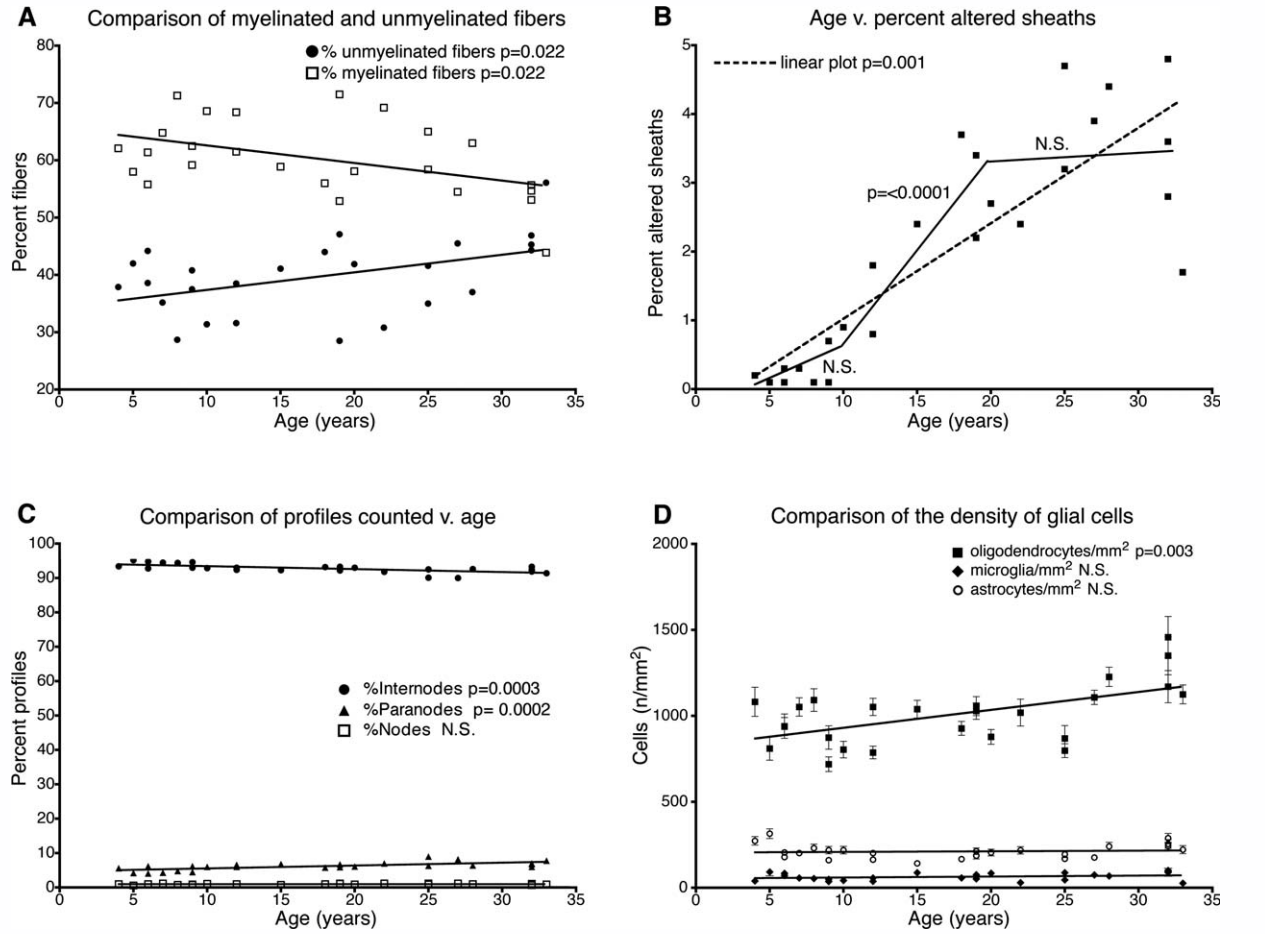

Figure 5. Graphs showing the effects of age on various morphological features of the fornix. **A:** Percentages of myelinated and of unmyelinated nerve fibers in the fornix as a function of age. **B:** Percentage of nerve fiber profiles showing alterations in the morphology of their myelin sheaths as a function of age. The dashed line shows the linear change in the frequency of altered sheaths with increasing age. The solid line is the piecewise plot, which shows that the most pronounced alterations in sheath morphology occur in middle age. **C:** Change in the percentages of nerve fiber profiles that belong to internodes, paranodes, and nodes of Ranvier as a function of age. **D:** Frequency of neuroglial cell profiles per square millimeter at increasing ages.

because such profiles are difficult to separate visually by light microscopy. In contrast, in electron micrographs, the profiles of individual nerve fibers are readily discernible (see Fig. 4).

Unmyelinated nerve fibers

The diameters of unmyelinated nerve fibers in the fornix range from about 0.6 μm to as small as 0.24 μm. The frequency of unmyelinated nerve fibers was determined in the electron microscopic analyses (see Figs. 5A, 6). It was found that in both young and middle aged monkeys the mean packing density of unmyelinated nerve fibers is 39 per 100 μm^2, whereas in old monkeys it is 38 fibers per 100 μm^2 (data for individual counts not given), which indicates that there is no change in the number of unmyelinated axons with age. In young monkeys unmyelinated nerve fibers account for about 38% of the total number of all nerve fiber profiles, and, because their numbers stay constant, although the frequency of myelinated nerve fibers decreases (Table 2), the numerical ratio between unmyelinated and myelinated nerve fibers in the fornix increases with age (Fig. 5A).

Age changes in myelinated nerve fibers

As we have shown in earlier studies (e.g., Feldman and Peters, 1998; Peters et al., 2000; Sandell and Peters, 2001; Peters and Sethares, 2002, 2003), four kinds of age-related changes affect the myelin sheaths of nerve fibers. Two of these changes are presumed to be degenerative. They are localized splitting of sheaths at the major dense line to accommodate electron-dense cytoplasm that is presumed to be derived from the

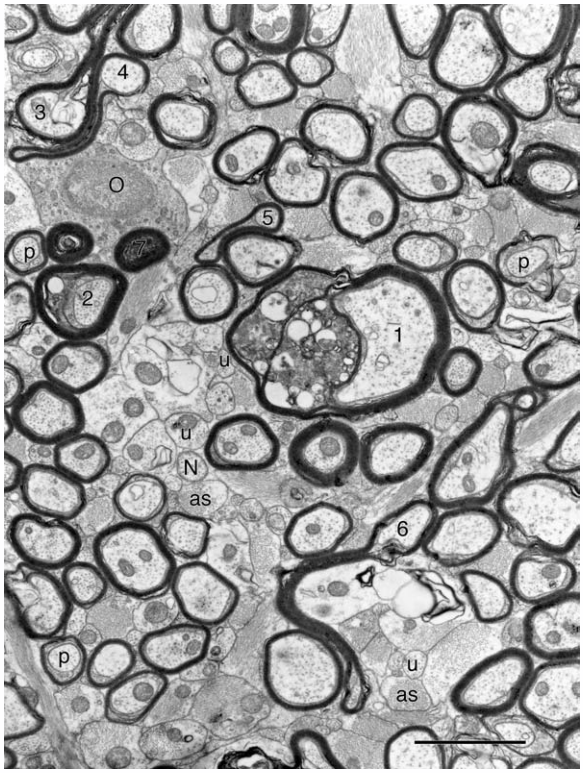

Figure 6. Electron micrograph from the fornix of a 19-year-old monkey (AM 133). In the field are two nerve fibers (1 and 2) with accumulations of dense cytoplasm in their myelin sheaths. A few other nerve fibers (3-6) have redundant myelin. Next to the oligodendroglial cell (O) is a nerve fiber (7) with a dense axon, indicating that it is degenerating. Some of the nerve fibers in the field are sectioned at paranodes (p), and one (N) has been sectioned through the node of Ranvier. Between the myelinated nerve fibers are some unmyelinated nerve fibers (u) and the processes of astrocytes (as). Scale bar = 2 μm.

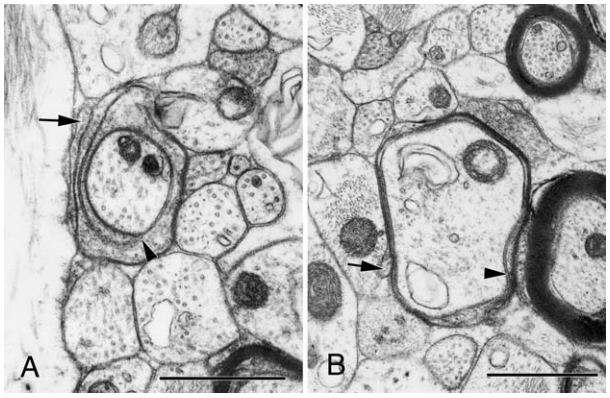

Figure 7. Remyelinating nerve fibers in the fornix of a 32-year-old monkey. **A:** This sheath is loose and has cytoplasm between the turns. The inner end of the spiral of lamellae is indicated by the arrowhead and the outer end by the arrow. This is not a section through a paranode, because there is a space between the axolemma and the inner membrane of the sheath. **B:** A thin myelin sheath consisting of two compact lamellae. The inner tongue process is indicated by the arrowhead and the outer tongue process by the arrow. Scale bars = 1 μm.

oligodendrocyte forming the sheath (see Fig. 6, 1 and 2) and, less commonly, the formation of fluid-filled blebs or balloons (see Fig. 2B) produced by splits of the intraperiod line. The other two age-related changes are produced by the continued formation of myelin with age. They are the formation of sheaths that have redundant myelin, so that the sheaths are too large for the enclosed axon (see Fig. 6, 3–6), and the increasingly common presence of thick myelin sheaths that show circumferential splitting.

The percentages of profiles of transversely sectioned myelinated nerve fibers showing such alterations in their sheaths are given in Table 2. In young monkeys profiles of few myelin sheaths (0.3%) show alterations, whereas the mean frequency increases to 2.4% in the middle-aged monkeys and increases further to 3.5% in the old monkeys. When the data for all monkeys are plotted in a linear manner (Fig. 5B, dashed line), it is found that there is a significant ($r = 0.839$, $P < 0.001$) increase in the frequency of occurrence of profiles of altered sheaths with increasing age. However, when a piecewise analysis is done (Fig. 5B, solid line), it becomes evident that the change with age in the frequency of altered sheaths in young monkeys and in old monkeys is not significant. However, there is a pronounced positive correlation association with age in the middle-aged group of monkeys ($P < 0.0001$), showing that the greatest increase in altered sheaths occurs between 10 and 20 years of age.

The frequencies of profiles of sheaths with redundant myelin and of sheaths with dense cytoplasm both increase with age, but overall the greatest increase in frequency is of sheaths with dense cytoplasm. Thus, in the fornices of young monkeys there are almost twice as many profiles of redundant sheaths as those of sheaths with dense cytoplasm, whereas in middle-aged monkeys the two kinds of profiles are equally frequent. However, in old monkeys there are almost five times more profiles of sheaths with dense cytoplasm than profiles of redundant sheaths.

There are also changes in the morphology of some of the axons of the myelinated nerve fibers. In middle-aged and in old monkeys some nerve fibers have degenerating axons with dense cytoplasm (Figs. 6, 7), and in others the sheaths are empty (Fig. 8A, d), indicating that their axons have degenerated. In middle-aged monkeys 0.2% of the axons are either dense or have degenerated, and the frequency increases to 0.3% in the old monkeys (Table 2). When a piecewise linear analysis is carried out, it becomes apparent that the significant association between age and the percentage of profiles of degenerating axons occurs in

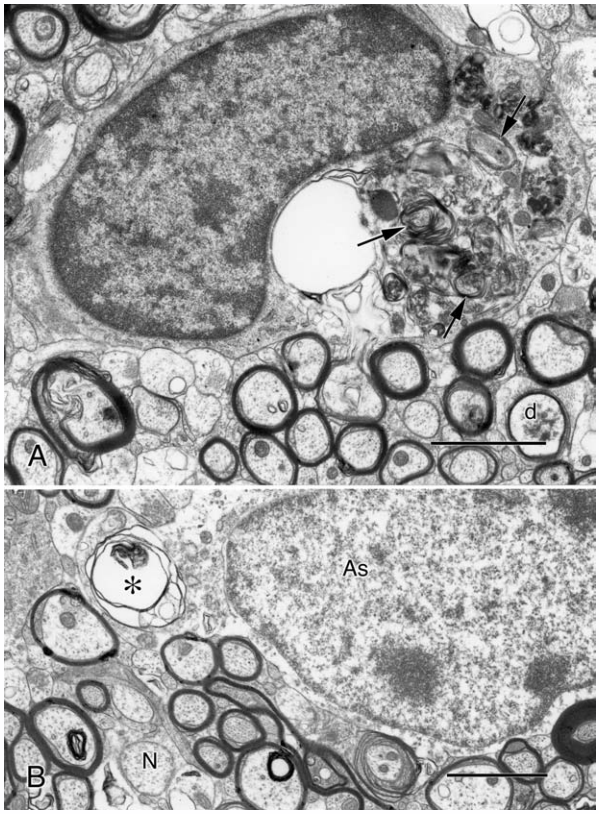

Figure 8. **A:** Microglial cell from a 32-year-old monkey (AM 91). The microglial cell has a bean-shaped nucleus, and its cytoplasm contains phagocytosed debris, some of which is laminated (arrows) and has the appearance of myelin. Note the degenerating nerve fiber, with a degenerated axon (d) in the lower right of the field. The fiber is surrounded by an astrocytic process. **B:** Part of an astrocyte (As) from a 32-year-old monkey (AM 23). The cytoplasm contains a laminated inclusion (asterisk), which has the appearance of phagocytosed myelin. Note the node of Ranvier (N) in the surrounding neuropil. Scale bars = 2 μm.

the middle-aged group of monkeys ($P < 0.01$), which coincides with the period when there is the greatest rate of increase in altered myelin sheaths (Fig. 5B).

Frequency of occurrence of profiles of internodes, paranodes, and nodes of Ranvier

In an earlier publication (Peters and Sethares, 2003) it was shown that, when all cross-sectioned profiles of myelinated nerve fibers in the vertical bundles that pass through primary visual cortex are considered, the frequency of occurrence of profiles of paranodes of myelinated axons increases with age. It was suggested that this is an indication that some remyelination of nerve fibers is taking place during aging. Paranodes occur at the ends of lengths, or internodes, of myelin, and at paranodes the lamellae of the myelin sheath gradually terminate in a spiral fashion (see Raine, 1984; Peters et al., 1991b; Rosenbluth, 1995). As described in the earlier publication (Peters and Sethares, 2003), and as illustrated in Figure 6, profiles of the paranodal portions of myelinated nerve fibers (Fig. 6, p) can be recognized because the axolemma and the membrane on the inside of the myelin sheath become apposed to form a junction in which these membranes are separated by only 3 nm. Because the lamellae terminate at paranodes, the portions of the axon between adjacent internodal lengths, that is, at the nodes of Ranvier, the axon is bare. At nodes, the axolemma has a distinctive electron-dense undercoating, which allows the profiles of nodal axons (Fig. 6, N) to be distinguished from those of unmyelinated axons (Fig. 6, u).

As shown in Table 2 and in Figure 5C, with increasing age there is a significant increase in the frequency of profiles of paranodes in the fornix ($r = 0.685$, $P < 0.0002$). As would be expected, there is also a concomitant decrease in the frequency of occurrence of profiles of internodes ($r = -0.658$, $P < 0.0003$), which for the present purposes are defined as the lengths of sheaths between paranodes. However, no change was detected in the frequency of occurrence of profiles of nodes of Ranvier, which may reflect the difficulty in distinguishing profiles of nodes from those of unmyelinated nerve fibers when the undercoating of the axolemma is not clearly evident.

Remyelination

Because there is an increase in the frequency of paranodal profiles with age, it is assumed that the mean lengths of internodes are decreasing, and this is taken to be an indication that some remyelination is taking place. It is generally agreed that the signs of remyelination are the occurrence of unusually thin myelin sheaths and of unusually short internodal lengths of myelin (see, e.g., Prineas and McDonald, 1997). Both were found in our earlier study of the effects of age on nerve fibers in the primary visual cortex of the monkey (Peters and Sethares, 2003). In the fornix of old monkeys, nerve fibers having sheaths consisting of loose lamellae with cytoplasm still between the turns of the sheath (Fig. 7A) and unusually thin sheaths consisting of only one or two lamellae are both encountered (Fig. 7B). These images are consistent with what would be expected for axons in the early stages of myelination.

Morphology of neuroglial cells

The three common types of neuroglial cells encountered in the fornix are oligodendrocytes, microglial cells, and astrocytes.

Oligodendrocytes are the most common type of neuroglial cell in the fornix. They can be recognized by their round nuclei, which stain densely and rather unevenly in both light (Fig. 2) and electron (Figs. 4) microscopic preparations. In electron microscopic preparations the dark perikaryal cytoplasm is seen to contain short, wide

cisternae of rough endoplasmic reticulum. There are many free ribosomes in the cytoplasm as well as numerous microtubules that come together in parallel bundles to enter the thin and dark processes that emanate from the cell body. In old monkeys these processes often form swellings that contain irregular and sometimes laminated dense inclusions (see Peters, 1996). These inclusions are characteristic of oligodendrocytes in old monkeys, and they also occur within the cell bodies.

Astrocytes have pale nuclei that are usually oval and larger than those of oligodendrocytes. Their cytoplasm is pale (Figs. 2, 4), and it is common to see quite thick processes extending from them. In thin sections, it is evident that these processes contain bundles of intermediate filaments (Fig. 6, as). With increasing age, the number of astrocytic processes become more abundant as they fill the spaces produced by degenerated nerve fibers. Concomitantly the concentration of intermediate filaments in the cytoplasm of astrocytes also increases. In addition, the perikaryal cytoplasm of astrocytes in old monkeys often contains inclusions, some of which are laminated, suggesting that they are derived from phagocytosed myelin (see Fig. 8B, asterisk).

Microglia are the least frequent of the neuroglial cells. As with the oligodendrocytes, their nuclei stain darkly, but the nuclei of the microglial cells are often oval, bean-shaped, or lobulated (Figs. 2, 8A). The microglial cells also have darkly staining cytoplasm, but they differ from oligodendrocytes in that their cisternae of rough endoplasmic reticulum are long. Also, overall, the shapes of the cells are irregular, because they mold themselves to the contours of the surrounding neuropil. With age, inclusions in the cytoplasm of microglial cells become increasingly common, and some of the inclusions have the appearance of phagocytosed myelin (Fig. 8A, arrows).

Changes in the frequency of neuroglial cells with age

The frequency of neuroglial cell profiles with nuclei, as determined by light microscopy, is given in Table 3. These data are also plotted in Figure 5D. In young monkeys oligodendrocytes account for about 77% of all neuroglial cell profiles, whereas 18% of the profiles belong to astrocytes and 5% to microglial cells. With age, there is no significant change in the frequency of occurrence of profiles of astrocytes and of microglial cells, but there is a significant increase, about a 20% increase, in the frequency of occurrence of oligodendroglial cell profiles ($r = 0.571$, $P < 0.0029$).

Correlations with behavior

Correlations were examined between CIIs and the following morphological measures: mean packing density of nerve fibers in the fornix measured by light and by electron microscopy, total numbers of myelinated nerve fibers in the fornix, percentages of altered myelin sheaths, frequency of occurrence of paranodes and nodes of Ranvier, and frequency of neuroglial cell profiles. There are three correlations between increasing cognitive impairment and morphological measures. They are between CII and the percentage of altered sheaths (Fig. 9A; $r = 0.411$, $P = 0.064$), CII and the percentage of altered axons (Fig. 9B; $r = 0.546$, $P = 0.0104$), and packing density of myelinated nerve fibers obtained by electron microscopic analyses (Fig. 9C; $r = 0.542$, $P = 0.015$). This result raises the question of why there is not a correlation between CII and the packing density of myelinated nerve fibers as determined by light microscopy. The most likely answer is that, as pointed out, the values for the packing densities obtained by electron microscopy, even though they were obtained from fields containing only myelinated nerve fibers and from only the lateral portion of the fornix, probably more accurately reflect the age-related changes in the population of myelinated nerve fibers than the measures obtained by light microscopy.

Correlations were also examined between each of the morphological measures and the scores made by monkeys on the individual behavioral components that are used to derive the CII values. The only correlations were between the mean packing densities of myelinated nerve fibers obtained by electron microscopy and both the DNMS task scores ($r = 0.493$, $P < 0.02$) and the scores for the DNMS task with a 2-minute delay (Fig. 9D; $r = 0.501$, $P < 0.024$).

DISCUSSION

Loss of nerve fibers with age

In electron micrographs of the fornices from both middle-aged and old monkeys, small numbers of myelinated nerve fibers are seen to have dark axons or empty myelin sheaths, indicating that some of the nerve fibers are degenerating. Consequently, when the total numbers of myelinated nerve fibers in the fornices of young and old monkeys are compared by light microscopy, it is found that old monkeys have lost some 15% of their myelinated nerve fibers. However, electron microscopic analyses of myelinated nerve fibers in the lateral portion of the fornix suggest that the loss may be even greater, insofar as their packing density decreases by about 34%. In other studies, we have also recorded age-related losses of myelinated nerve fibers from the optic nerves (Sandell and Peters, 2001), anterior commissure (Sandell and Peters, 2003), and corpus callosum (unpublished data), and there is reason to believe that nerve fiber loss from white matter is a ubiquitous feature of normal aging. This

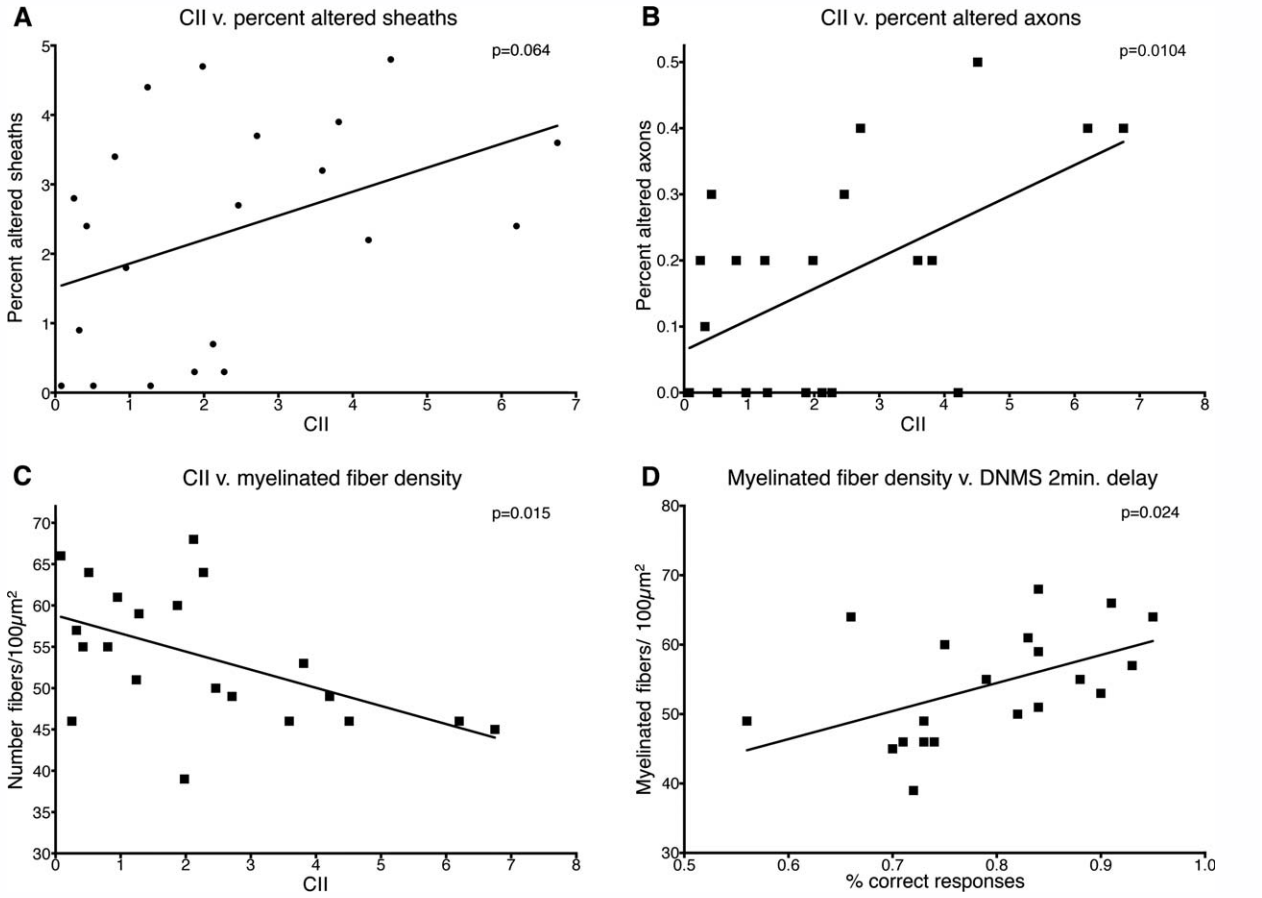

Figure 9. Correlations between morphological changes and cognition. **A:** Correlation between CII and the percentage of altered sheaths in the fornix. **B:** Correlation between CII and the percentage of altered axons. **C:** Correlation between CII and the packing density of myelinated nerve fibers as ascertained by electron microscopy. **D:** Correlation between the packing density of nerve fibers as determined by electron microscopy and the percentage of correct responses on the DNMS task with a 2-minute delay.

conclusion is supported by the only other quantitative studies of the effects of age on white matter, namely, the studies of Pakkenberg and coworkers. By using stereology, Pakkenberg and Gunderson (1997) determined that there is a 28% loss of white matter volume from human cerebral hemispheres with age, and Tang et al. (1997) and Marner et al. (2003) showed that this loss of white matter volume is due to a decrease in the total length of myelinated nerve fibers.

Why are nerve fibers lost?

There may be several reasons for the loss of myelinated nerve fibers from white matter. In the case of the optic nerve, the most likely explanation is that it results from degeneration of their parent ganglion cells in the aging retina (Garner et al., 1994). Loss of nerve fibers from the anterior commissure and corpus callosum requires a different explanation. Despite earlier reports that large numbers of neurons are lost from the neocortex of primates during normal aging (see Peters et al., 1998a), more recent studies have concluded that overall the age-reported neuronal loss from human and nonhuman primate neocortex is minimal (e.g., Pakkenberg and Gundersen, 1997; Morrison and Hof, 1997; Peters et al., 1998a; Hof et al., 2000; Merrill et al., 2000; Freeman et al., 2008), although Smith et al. (2004) have reported that there may be localized regions of prefrontal cortex, insofar as they find that as many as 32% of neurons are lost from area 8A with age.

The nerve fiber loss from the anterior commissure, which provides an interhemispheric connection for the temporal lobes, as well as parts of the orbitofrontal cortex, prepiriform cortex, and amygdala, is on the order of 45% (Sandell and Peters, 2003) and from the corpus callosum it is about 25% (unpublished data). It was proposed that these losses of nerve fibers are brought about not by a loss of cortical neurons but by selective degeneration of their long projecting axonal branches that enter white matter, the parent neuron being sustained by its

extensive local axonal plexus within the cortex (see, e.g., Feldman, 1984; Martin, 1988; Somogyi et al., 1998). There might be a similar explanation for the loss of nerve fibers from the fornix, although there have been some reports that neurons are lost from specific parts of the hippocampus. However, various studies on the aging primate hippocampus have reached conflicting conclusions. There have been reports of loss of neurons from the CA1 and subicular subfields of both humans (West and Gundersen, 1990) and monkeys (Brizzee et al., 1980), whereas West et al. (1994) detected a loss of neurons from the dentate hilus and subiculum of the human hippocampus, but not from the CA3-2 or CA1 regions. On the other hand, Simic et al. (1997) were not able to ascertain a loss of hilar neurons from the human brain, but they did report a loss of CA1 pyramidal cells with age, whereas Rosene (1993) and Amaral (1993) have reported that there is no loss of neurons with age from the monkey hippocampus. This conclusion has been substantiated by the study of Keuker et al. (2003), who found preservation of neuronal numbers in all parts of the aging rhesus monkey hippocampus.

If it is concluded that myelinated nerve fiber loss from white matter with age is not due to loss of the parent neurons from cerebral cortex or hippocampus, it has to be assumed that some factor, as yet unknown, causes degeneration in long projecting myelinated nerve fiber tracts. Whatever the cause, this loss of nerve fibers effectively results in some disconnection between groups of neurons, and this may be one of the underlying bases of the cognitive decline associated with normal aging. However, another contributing factor could be the age-related alterations that affect myelin sheaths and alter the conduction velocities along nerve fibers. Interestingly, although there is a loss of myelinated nerve fibers from the aging fornix, there does not appear to be a concomitant loss of unmyelinated nerve fibers.

Changes in myelin sheaths

The age-related changes in the myelin sheaths of nerve fibers in the fornix are similar to those we have encountered in other parts of the aging monkey brain, including area 17 of the cerebral cortex (Peters et al., 2000; Peters and Sethares, 2003), area 46 and corpus callosum (Peters and Sethares, 2002), optic nerve (Sandell and Peters, 2001), and anterior commissure (Sandell and Peters, 2003). Such alterations in myelin sheaths are not common in young monkeys, and our piecewise analyses show that age-related degenerative changes of myelin sheaths (Fig. 9), as well as of the frequency of nerve fibers with degenerating axons within the three age groups, are most pronounced in the fornices of middle-aged monkeys. On the other hand, the loss of nerve fibers with age (Fig. 3B,C) appears to continue in a steady fashion throughout life. A somewhat similar result was obtained in our analysis of the effects of age on the anterior commissure (Sandell and Peters, 2003), in which it was also found that alterations in the structure of myelin sheaths and the degeneration of axons begin and accelerate in middle age.

Paranodes

As in the fornix, it has been shown that with age there is an increase in the frequency of profiles of paranodes in both cerebral cortex (Peters and Sethares, 2003) and anterior commissure (Sandell and Peters, 2003). The increase in frequency of paranodal profiles cannot be explained on the basis of an increase in the lengths of paranodes with age (Peters and Sethares, 2003), and for this and other reasons it has been proposed that in the aging brain there is some breakdown and loss of some of the original internodal lengths of myelin, followed by remyelination of the bare lengths of axons with shorter internodal lengths of myelin. This would lead to a decrease in the average lengths of myelin internodes in the old monkeys and hence to an increase in the frequency of profiles of paranodes. In support of this conclusion, short internodal lengths of myelin have been found in the aging cerebral cortex, and, as in the fornix, some axons with inappropriately thin myelin sheaths have also been encountered. Both short internodes and inappropriately thin sheaths are generally considered to be the hallmarks of remyelination (see, e.g., Sethares and Peters, 2003).

Neuroglial cells

In the fornix, oligodendrocytes, which form the myelin sheaths of the central nervous system, account for about 77% of all neuroglial cell profiles. This is somewhat lower than the 86% that we encountered in the anterior commissure (Sandell and Peters, 2003). Both of these percentages of oligodendrocytes are higher than in optic nerve (60%; Sandell and Peters, 2002), in which there is a larger proportion of astrocytes. In optic nerve, astrocytes form the trabeculae of fibrous tissue that separate the nerve fibers into bundles, which are also surrounded by astrocytic sheaths. In the only gray matter that5 we have examined, the primary visual cortex, the percentage of oligodendrocytes is similar to that in optic nerve, namely, about 50% (Peters et al., 1991a; Peters et al., 2008). In each of these structures microglial cells consistently account for about 5–7% of the total numbers of neuroglia.

In the fornix there is a significant increase of about 20% in the frequency of oligodendrocytes with age (see Fig. 5D). In the optic nerve, on the other hand, there is a slight, nonsignificant, increase in the frequency of both

oligodendrocyte and of microglial cells with age (Sandell and Peters, 2002). This is in striking contrast to the 50% increase with age in the numbers of oligodendrocytes in primary visual cortex (Peters and Sethares, 2004; Peters et al., 2008).

It is presumed that the increase in the numbers of oligodendrocytes with age is related to the remyelination of some nerve fibers by short internodes. There appears to be little evidence that mature oligodendrocytes divide (see Ludwin, 1995; Norton, 1996; Keirstead and Blakemore, 1997), and the prevailing view is that in the mature brain any new oligodendrocytes are generated from the population of oligodendrocyte progenitors or precursor cells (see Norton, 1996; Levine et al., 2001; Chen et al., 2002; Watanabe et al., 2002; Rivers et al., 2008). These progenitor cells, which have a superficial resemblance to astrocytes (see Peters and Sethares, 2004; Peters, 2004), are present in all parts of the mature central nervous system.

In addition, as in other parts of the central nervous system, oligodendrocytes in the fornices of middle-aged and old monkeys come to accumulate dense inclusions in their cell bodies and processes. The origins of these dense inclusions are not yet known, but the oligodendrocytes that contain them might be those connected to the myelin sheaths showing the dense oligodendrocytic cytoplasm between their lamellae. The inclusions in the astrocytes and microglial cells, on the other hand, seem to be generated through phagocytosis, and the appearance of some of these inclusions suggests that at least one of the elements being phagocytosed is myelin (see Fig. 8). We have also encountered phagocytosis of myelin by microglial cells in the optic nerve (Sandell and Peters, 2002) and by astrocytes in the aging primary visual cortex (Peters and Sethares, 2003).

Cognitive performance

As pointed out above, correlations have been found between increasing cognitive impairment, as indicated by increasingly higher CII values, and three morphological assessments of the aging fornix. These morphological changes are the age-related increase in the number of profiles of altered myelin sheaths, the age-related increase in the numbers of profiles of degenerating axons, and the age-related decreasing density of myelinated nerve fibers as determined by electron microscopy. The correlation with cognitive impairment and the degeneration of myelin probably exists because such structural changes bring about reductions in the conduction velocities along myelinated nerve fibers (Aston-Jones et al., 1985; Morales et al., 1987; Xi et al., 1999), resulting in changes in the timing with which nerve impulses arising in the hippocampus reach their target structures. Similar correlations between cognitive impairment and age-related alterations in myelin sheaths have been encountered in the corpus callosum (unpublished data) but not in the anterior commissure (Sandell and Peters, 2001). However, for both primary visual cortex (Peters et al., 2000) and prefrontal cortical area 46 (Peters and Sethares, 2002), the correlations between cognitive impairment and myelin sheath alterations were stronger ($P < 0.001$) than in the fornix ($P = 0.064$), suggesting that changes in nerve conduction velocity along affected nerve fibers in the cortex, which probably affect intracortical neuronal processing, are more important to cognition than the transfer of data between various parts of the nervous system by long fiber tracts.

When correlations between morphological measures and the three behavioral components used to calculate the CII are examined, significant correlations are found between the mean packing density of nerve fibers, as determined by electron microscopy, and the scores of individual monkeys on the DNMS task and the DNMS task with a 2-minute delay (Fig. 9D). The DNMS task is a recognition memory task that assesses the ability of monkeys to identify a novel stimulus from a familiar stimulus, after a delay. The ability to perform this task successfully depends on the integrity of the hippocampus but not of the fornix (Mahut et al., 1982; Saunders et al., 1984; Zola-Morgan et al., 1989). It can be assumed, however, that a loss of nerve fibers from the fornix interferes with the efferent connections from the hippocampus, and it is not surprising that studies of the effects of damage to the fornix in both humans (e.g., Gaffan, 1974; Gaffan et al., 1991; D'Esposito et al., 1995) and monkeys (Owen and Butler, 1981; Gaffan et al., 2001; Wilson et al., 2007) have emphasized that the fornix has a role in memory and have described amnesia as the major consequence of lesions.

A speculation

A possible scenario that could account for the observations that we have made is that, by middle age, degeneration of myelin sheaths accelerates so that there is a reduction in the conduction velocity along those nerve fibers whose myelin sheaths are degenerating. The consequence is alterations of the precise timing in neuronal circuits that depend on the integrity of nerve fibers. Ultimately, the degenerating myelin is phagocytosed by astrocytes and microglial cells, and some of the desheathed axons are remyelinated by new and shorter lengths of myelin. This results in an increase in the frequency of profiles of paranodes. At the same time, some axons begin to degenerate in middle age, and this probably is due to degeneration of the long projecting branch of axonal plexuses of the cortical neurons, the local

axonal plexuses remaining largely intact. Consequently, some of the connections between the hippocampus and other structures of the brain are diminished, and this might contribute to the cognitive decline that occurs during normal aging in monkeys (see, e.g., Moss et al., 1999; Rosenzweig and Barnes, 2003). It may be added that, in normally aging old human brains, white matter changes are visible by magnetic resonance imaging, and it has also been proposed that the breakdown of white matter results in a disconnection that is the underlying cause of age-related cognitive decline in humans (De Groot et al., 2000; O'Sullivan et al., 2001; Madden et al., 2004). In any event, the age-related changes that occur in white matter are complex; they involve not only degeneration of both axons and their sheaths, with the consequent loss of nerve fibers, but also breakdown and loss of some myelin sheaths, followed by remyelination of the affected axons by new and shorter internodal lengths of myelin.

ACKNOWLEDGMENTS

We thank Dr. Douglas Rosene for carrying out the perfusions of the monkey brains, Dr. Howard Cabral for advice on statistical analyses and for carrying out the piecewise analyses of the data, and Dr. Tom Kemper for his comments on the manuscript.

LITERATURE CITED

Albert M. 1993. Neuropsychological and neurophysiological changes in healthy adult humans across the age range. Neurobiol Aging 14:623–625.

Amaral DG. 1993. Morphological analysis of the brains of behaviorally characterized aged nonhuman primates. Neurobiol Aging 14:671–672.

Andersen AH, Zhang Z, Zhang H, Gash DM, Avison MJ. 1990. Age-associated changes in rhesus CNS composition identified by MRI. Brain Res 829:90–98.

Aston-Jones G, Rogers J, Shaver RD, Dinan TG, Moss DE. 1985. Age-impaired impulse flow from nucleus basalis to cortex. Nature 318:462–464.

Brizzee KR, Ordy JM, Bartus, RT. 1980. Localization of cellular changes within multimodal regions of the aged monkey brain. Possible implications of age related cognitive loss. Neurobiol Aging 1:445–556.

Chen ZJ, Negra M, Levine A, Ughrin Y, Levine, JM. 2002. Oligodendrocyte precursor cells: reactive cells that inhibit axon growth and regeneration. J Neurocytol 31:481–495.

De Groot JC, de Leeuw F-E, Uodkerk M, van Gijn J, Hofman A, Joles J, Breteler M. 2000. Cerebral white matter lesions and cognitive function: the Rotterdam scan study Ann Neurol 47:145–151.

Demeter S, Rosene LR, van Hoesen GW. 1985. Interhemispheric pathways of the hippocampal formation, presubiculum, and entorhinal and posterior parahippocampal cortices in the rhesus monkey: the structure and organization of the hippocampal commissures. J Comp Neurol 233: 30–47.

D'Esposito M, Verfaellie M, Alexander, MP, Katz DI. 1995. Amnesia following traumatic bilateral fornix transection. Neurology 45:1546–1550.

Duan H, Wearne SL, Rocher AB, Macedo A, Morrison JH, Hof PR. 2003. Age-related dendritic and spine changes in corticocortical projecting neurons in macaque monkeys. Cerbr Cortex 13:950–961.

Feldman ML. 1984. Morphology of the neocortical pyramidal neuron. In: Peters A, Jones EG, editors. Cellular components of the cerebral cortex. Cerebral cortex, vol 1. New York: Plenum Press. p 123–200.

Feldman ML, Peters A. 1998. Ballooning of myelin sheaths in normally aged macaques. J Neurocytol 27:605–614.

Freeman SH, Kandel R, Cruz L, Rozkalne A, Newell K, Frosch MP, Hedley-White T, Locascio JJ, Lipsitz LA, Hyman BT. 2008. Preservation of neuronal number despite age-related cortical brain atrophy in elderly subjects without Alzheimer disease. J Neuropathol Exp Neurol 67: 1205–1212.

Gaffan D. 1974. Recognition impaired and association intact in the memory of monkeys after transection of the fornix. J Comp Physiol Psychol 86:1100–1109.

Gaffan EA, Gaffan D, Hodges JR. 1991. Amnesia following damage to the left fornix and to other sites. A comparative study. Brain 114:1297–1313.

Gaffan, D, Parker A, Easton A. 2001. Dense amnesia in the monkey after transection of fornix, amygdala and anterior temporal stem. Neuropsychologica 39:51–70.

Garner A, Sarks S, Sarks JP. 1994. Degenerative and related disorders of the retina and choroid. In: Garner A, Klintworth GK, editors. Pathobiology of ocular disease. New York: Marcel Dekker. p 631–674.

Guttman CRG, Jolesz FA, Kikinis R, Killiany RJ, Moss MB, Sandor T, Albert MS. 1998. White matter changes with normal aging. Neurology 50:972–978.

Herndon J Moss MB, Killiany RJ, Rosene DL. 1997. Patterns of cognitive decline in early, advanced and oldest of the old aged rhesus monkey. Behav Res 87:25–34.

Hof RP, Nimchinsky EA, Young W, Morrison JH. 2000. Numbers of Meynert and layer IVB cells in area V1; stereological analysis in young and aged macaque monkeys. J Comp Neurol 420:113–126.

Howard C, Reed MG. 1998. Unbiased stereology: three dimensional measurement in microscopy. New York: Springer-Verlag.

Jabobs B, Driscoll L, Schall M. 1997. Life-span dendritic and spine changes in area 10 and 18 of human cortex: a quantitative Golgi study. Cereb Cortex 11:558–571.

Johnston D, Amaral DG. 1998. Hippocampus. In: Shepherd GM, editor. The synaptic organization of the brain, 4th ed. New York: Oxford University Press. p 417–458.

Keirstead HS, Blakemore WF. 1997. Identification of post-mitotic oligodendrocytes incapable of remyelination with the demyelinated adult spinbal cord. J Neuropathol Exp Neurol 56:1191–1201.

Kemper TL. 1994. Neuroanatomical and neuropathological changes during aging and dementia. In: Albert ML, Knoefel JE, editors. Clinical neurology of aging. New York: Oxford University Press. p 3–67.

Keuker JIH, Luiten PGM, Fuchs E. 2003. Preservation of hippocampal neuron numbers in aged rhesus monkeys. Neurobiol Aging 24:157–165.

Killiany RJ, Moss MB, Rosene DL, Herndon J. 2000. Recognition memory function in early senescent rhesus monkeys. Psychobiology 28:45–56.

Lai ZC, Rosene DL, Killiany RJ, Pugliese D, Albert MS, Moss MB. 1995. Age-related changes in the brain of the rhesus monkey. MRI changes in white matter but not gray matter. Soc Neurosci Abstr 21:1564.

Levine JM, Reynolds R, Fawcett JW. 2001. The oligodendrcoyte precursor cell in health and disease. Trends Neurosci 24:39–47.

Lintl P, Braak H. 1983. Loss of intracortical myelinated fibers: a distinctive alteration in the human striate cortex. Acta Neuropathol 61:178–182.

Ludwin SK. 1995. Pathology of the myelin sheath. In: Waxman SG, Kocsis JD, Stys PK, editors. The axon: structure, function and pathophysiology. New York: Oxford University Press. p 412–437.

Madden DJ, Whiting WL, Huettel SA, White LE, MacFall JR, Provenzale JM. 2004. Diffusion tensor imaging of adult age differences in cerebral white matter: relation to response time. NeuroImage 21:1174–1181.

Mahut H, Zola-Morgan S, Moss MB. 1982. Hippocampal transections impair associative learning and recognition memory in the monkey. J Neurosci 2:1214–1229.

Marner L, Nyengaard JR, Tang Y, Pakkenberg B. 2003. Marked loss of myelinated nerve fibers in the human brain with age. J Comp Neurol 144–152.

Martin K. 1988. From single cells to simple circuits in the cerebral cortex. Q J Exp Physiol 73:637–702.

Merrill SM, Roberts JA, Tuszynski MH. 2000. Conservation of neuron number and size in entorhinal cortex layers II, III, and V/VI of aged primates. J Comp Neurol 422:396–401.

Morales FR, Boxer PA, Fung SJ, Chase MH. 1987. Basic electrophysiological properties of spinal cord motoneurons during old age in the cat. J Neurophysiol 58:180–194.

Morrison JH, Hof PR. 1997. Life and death of neurons in the aging brain. Science 278:412–419.

Moss MB, Killiany RJ, Herdon JG. 1999. Age-related cognitive decline in rhesus monkey. In: Peters A, Morrison JH, editors. Neurodegenerative and age-related changes in structure and function of the cerebral cortex. New York: Cerebral cortex, vol 14. New York: Kluwer Academic/Plenum Publishers. p 21–48.

Nielsen K, Peters A. 2000. The effects of aging on the frequency of nerve fibers in rhesus monkey striate cortex. Neurobiol Aging 21:621–628.

Norton WT. 1996. Do oligodendrocytes divide? Neurochem Res 21:495–503.

Owen NJ, Butler SR. 1981. Amnesia after transection of the fornix in monkeys; long-term memory impaired, short-term memory intact. Behav Brain Res 3:115–123.

O'Sullivan M, Jones DK, Summers PE, Morris RG, Williams SCR, Markus HS. 2001. Evidence for cortical "disconnection" as a mechanism of age-related cognitive decline. Neurology 384:312–320.

Pakkenberg B, Gundersen HJG. 1997. Neocortical neuron numbers in humans: effect of sex and age. J Comp Neurol 384:312–320.

Peters A. 1996. Age-related change in oligodendrocytes in monkey cerebral cortex. J Comp Neurol 371:152–163.

Peters A. 2004. A fourth type of neuroglial cell in the adult central nervous system. J Neurocytol 33:345–357.

Peters A, Sethares C. 2002. Aging and the myelinated fibers in prefrontal cortex and corpus callosum of the monkey. J Comp Neurol 442:277–291.

Peters A, Sethares C. 2003. Is there remyelination during aging of the primate central nervous system? J Comp Neurol 460:238–254.

Peters A, Sethares C. 2004. Oligodendrocytes, their progenitors and other neuroglial cells in the aging primate cerebral cortex. Cereb Cortex 14:995–1007.

Peters A, Josephson K, Vincent SL. 1991a. Effects of aging on the neuroglial cells and pericytes within area 17 of the rhesus monkey cerebral cortex. Anat Rec 229: 384–398.

Peters A, Palay SL, Webster DeFH. 1991b. The fine structure of the nervous system. Neurons and their supporting cells. New York: Oxford University Press.

Peters A, Leahu D, Moss MB, McNally KJ. 1994. The effects of aging on area 46 of the frontal cortex of the rhesus monkey. Cereb Cortex 6:621–635.

Peters A, Rosene DL, Moss MB, Kemper TL, Abraham CR, Tigges J, Albert MS. 1996. Neurological bases of age-related cognitive decline in the rhesus monkey. J Neuropathol Exp Neurol 55:861–874.

Peters A, Morrison JH, Rosene DL, Hyman BT. 1998a. Are neurons lost from the primate cerebral cortex during normal aging? Cereb Cortex 8:295–300.

Peters A, Sethares C, Moss MB. 1998b. The effects of aging on layer 1 in area 46 of pefrontal cortex in the rhesus monkey. Cereb Cortex 8:671–684.

Peters A, Moss MB, Sethares C. 2000. Effects of aging on myelinated nerve fibers in monkey primary visual cortex. J Comp Neurol 419:364–376.

Peters A, Moss MB, Sethares C. 2001a. The effects of aging on layer 1 of primary visual cortex in the rhesus monkey. Cereb Cortex 11:93–103.

Peters A, Sethares C, Killiany RJ. 2001b. Effects of age on the thickness of myelin sheaths in monkey primary visual cortex. J. Comp Neurol 435:241–248.

Peters A, Verderosa A, Sethares C. 2008. The neuroglial population in the primary visual cortex of the aging rhesus monkey. Glia 56:1151–1161.

Pfefferbaum A, Mathalon DH, Rawles JM, Zipursky RB, Lim KO. 1994. A quantitative magnetic resonance study of changes in brain morphology from infancy to late adulthood. Arch Neurol 9:874–887.

Poletti CE, Creswell G. 1977. Fornix system efferent projections in the squirrel monkey: an experimental degeneration study. J Comp Neurol 175:101–127.

Prineas JW, McDonald WI. 1997. Demyelinating diseases. In: Graham DI, Lantos PL, editors. Greenfield's neuropathology, 6th ed. London: Arnold. p 813–896.

Raine CS. 1984. Morphology of myelin and myelination In: Morell P, editor. Myelin. New York: Plenum Press. p 1–50.

Rivers, LE, Young KM, Rizzi M, Jamen F, Psachoulia K, Wade A, Kessaris N, Richardson WD. 2008. PDGFRA/NG2 glia generate myelinating oligodendrocytes and piriform projection neurons in adult mice. Nat Neurosci 11:1392–1401.

Rosenbluth J. 1995. Glial membranes and axoglial junctions. In: Waxman SG, Kocsis JD, Sytys PK, editors. The axon: structure, function and pathophysiology. New York. Oxford University Press. p 613–633.

Rosene DL. 1993. Comparing age-related changes in the basal forebrain and hippocampus of the rhesus monkey. Neurbiol Aging 14:669–670.

Rosene DL, van Hoesen G. 1987. The hippocampal formation of the primate brain. A review of some comparative aspects of cytoarchitecture and connections. In: Jones EG, Peters A, editors. Further aspects of cortical function, including hippocampus. Cerebral cortex, vol 6. New York: Plenum Press. p 345–456.

Rosenzweig ES, Barnes CA. 2003. Impact of aging on hippocampal function: plasticity, network dynamics, and cognition. Prog Neurobiol 69:143–179.

Sandell JH, Peters A. 2001. Effects of age on nerve fibers in the rhesus monkey optic nerve. J Comp Neurol 429:541–553.

Sandell JH, Peters A. 2002. Effects of age on the glial cells in the rhesus monkey optic nerve. J Comp Neurol 445: 13–28.

Sandell JH, Peters A. 2003. Disrupted myelin and axon loss in the anterior commissure of the aged rhesus monkey. J Comp Neurol 466:14–30.

Saunders RC, Murray EA, Mishkin M. 1982. Further evidence that the amgydala and hippocampus contribute equally to recognition memory. Neuropsychologia 22:758–796.

Siddiqi ZA, Peters A. 1999. The effect of age on pars compacta of the substantia nigra in rhesus monkey. J Neuropathol Exp Neurol 58:903–920.

Simic G, Kostovic I, Winblad B, Bogdanovic N. 1997. Volume and number of neurons in the human hippocampal formation in normal aging and Alzheiner's disease. J Comp Neurol 379:482–494.

Smith DE, Rapp PR, McKay HM, Roberts KA, Tuszynski MH. 2004. Memory impairment in aged primates is associated with focal death of cortical neurons and atrophy of subcortical neurons. J Neurosci 24:4373–4381.

Somogyi P, Tamas G, Lujan R, Buhl EH. 1998. Salient features of synaptic organisation in the cerebral cortex. Brain Res Revs 26:113–135.

Swanson LW, Cowan WM. 1977. An autoradiographic study of the organization of the efferent connections of the hippocampal formation in the rat. J Comp Neurol 172: 49–84.

Tang Y, Nyengaard JR, Pakkenberg G, Gundersen JJG. 1997. Age-induced white matter changes in the human brain: a stereological investigation. Neurobiol Aging 18:609–615.

Watanabe M, Toyama Y, Nishiyama A. 2002. Differentiation of proliferating NG2-positive glial progenitor cells in a remyelinating lesion. J Neurosci Res 69:826–836.

West MJ, Gundersen HJG. 1990. Unbiased stereological estimation of the number of neurons in the human hippocampus. J Comp Neurol 296:1–22.

West MJ, Coleman PD, Flood DG, Troncoso JC. 1994. Differences in the pattern of hippocampal neuronal loss in normal ageing and Alzheimer's disease. Lancet 344:769–672.

West MJ, Ostergaard K, Anreassen OA, Finsen B. 1996. Estimation of the number of somatostatin neurons in striatum: an in situ hybridization study using the optical fractionator method. J Comp Neurol 370:11–22.

Wilson, CRE, Charles DP, Buckley NJ, Gaffan D. 2007. Fornix transection impairs learning of randomly changing object discriminations. J Neurosci 21:12868–12873.

Wisco JJ, Killiany RJ, Guttmann CRG, Warfield SK, Moss MB, Rosene DL. 2008. An MRI study of age-related white and gray matter volume changes in the rhesus monkey. Neurobiol Aging 10:1563–1575.

Xi M-C, Lui R-H, Englehardt KK, Morales FR, Chase MH. 1999. Changes in the axonal conduction velocity of pyramidal tract neurons in the aged cat. Neuroscience 92:219–225.

Zola-Morgan S, Squire LR, Amaral DG. 1989. Lesions of the hippocampal formation, but not lesions of the fornix of the mammillary nuclei, produce long-lasting memory impairment in monkey. J Neurosci 9:898–913.